 CMES, vol.94, no.3, pp.239-260, 2013

On Macroscopic Behaviors of Shape Memory Alloy Thick-walled Cylinder Under Combined Internal Pressure and Radial Temperature Gradient

Bingfei Liu[1], **Guansuo Dui**[2,3], **Lijun Xue**[2], **Benming Xie**[1]

Abstract: Analytical solutions are derived for the macroscopic behaviors of a Shape Memory Alloy (SMA) thick-walled cylinder subjected to internal pressure and radial temperature gradient. The Tresca transformation criterion and linear hardening are used. Equations are given for the radial and circumferential stresses, transformation strains and martensite volume fractions at both the elastic step and the transformation step. Numerical results are presented and in good agreement with the finite element simulations.

Keywords: Shape memory alloy; Temperature gradient; Constitutive model

1 Introduction

Over the last two decades, as a new type of functional materials, Shape Memory Alloys (SMAs) have been utilized in various fields such as aerospace [Liang, Davidson, Scjetky and Straub (1996)] naval [Garner, Wilson, Lagoudas and Rediniotis (2000)] biomedical applications such as surgical instruments [Ilyin Dudin and Makarova (1995)] medical implants [Martynova and Savi (1991)] and fixtures [Gyunter, Wilson, Lagoudas and Rediniotis (1995)] due to their interesting behaviors such as the shape memory effect, superelasticity and biocompatibility. Due to this interest, this list of SMA applications continues to expand

As the number and complexity of SMA applications has grown, so has the need for models capable of capturing the unique behavior of SMAs. The study of SMA constitutive models has been the subject of a number of research papers [Müller and Xu (1991); Boyd and Lagoudas (1996); Lagoudas, Bo and Qidwai (1996); Qidwai and Lagoudas (2000); Müller and Seelecke (2001); Kim, Jang and Choi (2002);

[1] Airport College, Civil Aviation University of China, Tianjin, 300300, China.
[2] Institute of Mechanics, Beijing Jiaotong University, Beijing 100044, China.
[3] Corresponding author. Tel.: +1-86-1051688437; fax: +1-86-1051682094.
Email: Gsdui@center.njtu.edu.cn

Machado and Savi (2003); Langelaar and Keulen (2004); Kuribayashi, Tsuchiya, You, Tomusb, Umemorob, Ito and Sasaki (2006); Auricchio, Conti, Morganti and Reali (2010); Mirzaeifar, Shakeri, DesRoches and Yavari (2011); Liu, Dui and Zhu (2011, 2012); Chen, Peng, Chen, Wang, Wang and Hu (2012); Tablesh, Atli, Rohmer, Franco, Karaman, Boyd and Lagoudas (2012)]. Among various shapes in which SMAs are used, the SMA cylindrical shells are of particular interest in applications including spinal vertebrae spacers Machado and Savi (2003), special cardiovascular stents [Kuribayashi, Tsuchiya, You, Tomusb, Umemorob, Ito and Sasaki (2006)], and active catheters [Langelaar and Keulen (2004)], which are in the form of thin shells Due to easiness in installation and their ability to resist temperature the form of thick shells such as SMA short cylinders or rings has many engineering applications, e.g. the SMA pipe couplings [Jee, Hana and Jang (2006); Tablesh, Atli, Rohmer, Franco, Karaman, Boyd and Lagoudas (2012)], tube wall joints [Xua and Song (2004)], and active stiffener strips [Kim, Jang and Choi (2002)] Replacing current steel pressure vessel designs with polymer matrix composite pressure vessels for high pressure applications will yield significant weight reductions and can reduce the size and weight of fuel, hydraulic and auxiliary systems. An investigation of adaptive long thick composite cylinders utilizing active SMA composite layers for use in high-pressure vessel application is presented in Paine, Rogers and Smith (1995)

As for the research of thin shells, Li and Sun (2002) studied the superelastic response of nano-grained SMA microtubes under uniaxial tension. Their experimental results show that the nucleated macroscopic martensite band in a microtube under uniaxial loading takes the shape of a spiral that surrounds the tube axis for several circles. Feng and Sun (2007) studied the response of SMA microtubes subjected to a combined tensile and torsional loading experimentally. He and Sun (2009) studied the effect of tube geometry on the helix-shaped deformation domains that are observed in SMA tubes during the stress-induced martensitic phase transformation of the material under uniaxial stretching. As for the thick-walled cylinders made of SMAs, Mirzaeifar, Shakeri, DesRoches and Yavari (2011) analyzed the pseudoelastic response of a thick-walled SMA cylinder subjected to internal pressure for both plane strain and plane stress conditions. The cylinder was partitioned into a finite number of annular regions and closed-form solutions were provided for the equilibrium equations in each annulus. The global solution was obtained by enforcing stress continuity at the interface of the annular regions and by numerically solving the system of algebraic equations derived. The solutions were in excellent agreement with the results of a finite element analysis. A SMA pipe coupler was designed, fabricated and tested in Tablesh, Atli, Rohmer, Franco, Karaman, Boyd and Lagoudas (2012). Two alloy systems are

considered: commercially-available NiTiNb couplers and in-house developed NiTi couplers. The coupling pressure is measured and an axisymmetric finite element model including SMA constitutive equations is also developed Tabesh Liu, Boyd and Lagoudas (2013) also presented an analytical solution for the pseudoelastic response of a shape memory alloy (SMA) thick-walled cylinder subjected to internal pressure. The behaviors of such materials under combined internal pressure and radial temperature gradient, however, was not discussed

In the current work, the analytical solution of the pseudoelastic response of SMA thick-walled cylinders subjected to internal pressure and radial temperature gradient is presented. It is wellknown that under tensile loads, SMAs exhibit inhomogeneous deformations, and coupling the problem with temperature, of course, makes the solution even more complex. In order to get the analytical solution, a thermodynamically constitutive model for SMAs is developed that incorporates the Tresca transformation criterion, associated flow rule and linear hardening. This model is simplified for the assumptions of plane stress and plane strain in the SMA cylinder. The Tresca flow rule requires the transformation strain to be equal and opposite in the circumferential and radial directions, thereby enabling a closed-form solution for the equilibrium equation. The radial and circumferential stresses, transformation strains and volume fractions of martensite are obtained and compared with the finite element simulations

2 Constitutive model for NiTi SMA cylinder

According to Boyd and Lagoudas (1996) and Qidwai and Lagoudas (2000), the Gibbs free energy for an SMA material as a function of Cauchy stress tensor σ, temperature T and a set of internal variables γ is give in the following form:

$$\begin{aligned} G(\boldsymbol{\sigma}, T, \varepsilon^{\mathbf{t}}, \xi) = &-\frac{1}{2\rho}\boldsymbol{\sigma} : \mathbf{S} : \boldsymbol{\sigma} - \frac{1}{\rho}\boldsymbol{\sigma} : [\boldsymbol{\alpha}(T - T_0) + \boldsymbol{\varepsilon}^{\mathbf{t}}] \\ &+ c[T - T_0 - T\ln\frac{T}{T_0}] - s_0 T + G_0 + \frac{1}{2\rho}\eta\boldsymbol{\varepsilon}^{\mathbf{t}} : \boldsymbol{\varepsilon}^{\mathbf{t}} \end{aligned} \tag{1}$$

where $\mathbf{S}$ is the compliance tensor, $\boldsymbol{\alpha}$ is the coefficient of thermal expansion tensor, ρ is the material density, c is the specific heat s_0 and G_0 are the values of entropy and Gibbs energy at a reference state, the subscript '0' represents the reference state and η is the hardening modulus. We assume that the elastic compliance, thermal expansion, and specific heat are the same for the austenite and martensite phases. The entropy and reference energy are written using the rule of mixtures as:

$$\begin{aligned} s_0(\xi) &= s_0^A + \xi(s_0^M - s_0^A) \\ G_0(\xi) &= G_0^A + \xi(G_0^M - G_0^A) \end{aligned} \tag{2}$$

The set of internal variables contains the transformation strain tensor $\boldsymbol{\varepsilon}^{\mathbf{t}}$ and martensite volume fraction ξ to represent the changes in the microstructure of the material is

$$\boldsymbol{\gamma} = \{\boldsymbol{\varepsilon}^{\mathbf{t}}, \xi\} \tag{3}$$

The second law of thermodynamics in terms of Clausius-Planck inequality is

$$-\rho\dot{G} - \rho s\dot{T} - \boldsymbol{\varepsilon} : \dot{\boldsymbol{\sigma}} \geq 0 \tag{4}$$

Using the chain rule with G, we have

$$-(\rho\frac{\partial G}{\partial \boldsymbol{\sigma}} + \boldsymbol{\varepsilon}) : \dot{\boldsymbol{\sigma}} - \rho(\frac{\partial G}{\partial T} + s) : \dot{T} - \rho\frac{\partial G}{\partial \boldsymbol{\gamma}} : \dot{\boldsymbol{\gamma}} \geq 0 \tag{5}$$

The existence of a thermoelastic loading path with independent stress and temperature rates along which the second law inequality has to be satisfied implies that

$$\sim \varepsilon = -\rho\frac{\partial G}{\partial \sigma} \quad \text{and} \quad s = -\frac{\partial G}{\partial T} \tag{6}$$

Therefore the constitutive relations for the SMA material will be

$$\begin{aligned} \boldsymbol{\varepsilon} &= \mathbf{S} : \boldsymbol{\sigma} + \boldsymbol{\alpha}(T - T_0) + \boldsymbol{\varepsilon}^{\mathbf{t}} \\ s &= \tfrac{1}{\rho}\boldsymbol{\sigma} : \boldsymbol{\alpha} + c\ln(\tfrac{T}{T_0}) + s_0 \end{aligned} \tag{7}$$

This explicitly results in additive decomposition of strains

$$\boldsymbol{\varepsilon}^{\mathbf{e}} = \boldsymbol{\varepsilon} - \boldsymbol{\alpha}(T - T_0) - \boldsymbol{\varepsilon}^{t} \tag{8}$$

Based on the reduced form of the second law, a transformation dissipation potential is defined to be given by

$$D^t = -\rho\frac{\partial G}{\partial \boldsymbol{\gamma}} : \dot{\boldsymbol{\gamma}} \geq 0 \quad \text{with} \quad \boldsymbol{\Gamma} = \text{-}\rho\frac{\partial G}{\partial \boldsymbol{\gamma}} \quad \text{then} \quad \boldsymbol{\Gamma} : \dot{\boldsymbol{\gamma}} \geq 0 \tag{9}$$

Then the following generalized forces can be defined

$$\boldsymbol{\sigma}^{\mathbf{eff}} = -\rho\frac{\partial G}{\partial \boldsymbol{\varepsilon}^{\mathbf{t}}} = \boldsymbol{\sigma} - \eta\boldsymbol{\varepsilon}^{\mathbf{t}} \tag{10}$$

$$\boldsymbol{\Theta} = -\rho\frac{\partial G}{\partial \xi} = \rho\Delta s_0 T - \rho\Delta G_0 \tag{11}$$

where $\Delta s_0 = s_0^M - s_0^A$, $\Delta G_0 = G_0^M - G_0^A$ the superscripts A and M denote the austenitic and martensitic phases, respectively The terms with Δindicate the difference of the corresponding quantity in martensite and austenite phases

It is assumed that a transformation function exists that defines the boundary of the thermoelastic region as

$$\varphi(\mathbf{\Gamma}) = \varphi(\boldsymbol{\sigma}^{\mathbf{eff}}, \mathbf{\Theta}) = 0 \tag{12}$$

Within which all admissible material states, thermoelastic or transforming obey

$$\varphi(\mathbf{\Gamma}) = \varphi(\boldsymbol{\sigma}^{\mathbf{eff}}, \mathbf{\Theta}) \leq 0 \tag{13}$$

Application of the principle of maximum transformation dissipation results in the transformation evolution equations and Kuhn-Tucker conditions as below

$$\dot{\varepsilon}^t = \lambda \frac{\partial \varphi}{\partial \boldsymbol{\sigma}^{\mathbf{eff}}} \quad \text{and} \quad \dot{\xi} = \lambda \frac{\partial \varphi}{\partial \mathbf{\Theta}} \tag{14}$$

$$\lambda \geq 0,\ \varphi(\boldsymbol{\sigma}^{\mathbf{eff}}, \mathbf{\Theta}) \leq 0,\ \lambda \varphi(\boldsymbol{\sigma}^{\mathbf{eff}}, \mathbf{\Theta}) = 0 \tag{15}$$

We can conclude that

$$\dot{\boldsymbol{\varepsilon}}^{\mathbf{t}} = \dot{\xi} \frac{1}{\frac{\partial \varphi}{\partial \mathbf{\Theta}}} \frac{\partial \varphi}{\partial \boldsymbol{\sigma}^{\mathbf{eff}}} \tag{16}$$

Therefore the transformation dissipation potential will be

$$D^t = \mathbf{\Gamma} : \dot{\boldsymbol{\gamma}} = \boldsymbol{\sigma}^{\mathbf{eff}} : \dot{\boldsymbol{\varepsilon}}^{\mathbf{t}} + \mathbf{\Theta}\dot{\xi} = (\frac{1}{\frac{\partial \varphi}{\partial \mathbf{\Theta}}} \boldsymbol{\sigma}^{\mathbf{eff}} : \frac{\partial \varphi}{\partial \boldsymbol{\sigma}^{\mathbf{eff}}} + \mathbf{\Theta})\dot{\xi} = \pi \dot{\xi} \geq 0 \tag{17}$$

where π is the generalized thermodynamic force conjugate to martensite volume fraction ξ. A general form for the transformation function, it is proposed that

$$\varphi(\mathbf{\Gamma}) = \varphi(\boldsymbol{\sigma}^{\mathbf{eff}}, \mathbf{\Theta}) = [\hat{\varphi}(\boldsymbol{\sigma}^{\mathbf{eff}}) + \mathbf{\Theta}]^2 - Y^2 \tag{18}$$

where Y is a measure of internal dissipation due to microstructural changes during phase transformation, therefore

$$\begin{aligned} \dot{\boldsymbol{\varepsilon}}^{\mathbf{t}} &= 2\lambda [\hat{\varphi}(\boldsymbol{\sigma}^{\mathbf{eff}}) + \mathbf{\Theta}] \frac{\partial \hat{\varphi}(\boldsymbol{\sigma}^{\mathbf{eff}})}{\partial \mathbf{\Theta}} \\ \dot{\xi} &= 2\lambda [\hat{\varphi}(\boldsymbol{\sigma}^{\mathbf{eff}}) + \mathbf{\Theta}] \end{aligned} \tag{19}$$

From the equations above we can conclude that

$$\dot{\boldsymbol{\varepsilon}}^{\mathbf{t}} = \dot{\xi} \frac{\partial \hat{\varphi}(\boldsymbol{\sigma}^{\mathbf{eff}})}{\partial \boldsymbol{\sigma}^{\mathbf{eff}}} \tag{20}$$

Applying the Kuhn-Tucker conditions in equation (14-15) on the general form of the transformation function (18) results in

$$\begin{cases} \dot{\boldsymbol{\varepsilon}}^t = \dot{\xi}\dfrac{\partial\hat{\varphi}(\boldsymbol{\sigma}^{eff})}{\partial\boldsymbol{\sigma}^{eff}} \\ \varphi(\boldsymbol{\sigma}^{eff},\boldsymbol{\Theta}) \le 0 \quad \Rightarrow \quad -Y \le \hat{\varphi}(\boldsymbol{\sigma}^{eff}) + \boldsymbol{\Theta} \le Y \\ \dot{\xi} \ne 0 \Rightarrow \varphi(\boldsymbol{\sigma}^{eff},\boldsymbol{\Theta}) = 0 \Rightarrow \begin{cases} \hat{\varphi}(\boldsymbol{\sigma}^{eff}) + \boldsymbol{\Theta} = Y & forward \\ \hat{\varphi}(\boldsymbol{\sigma}^{eff}) + \boldsymbol{\Theta} = -Y & reverse \end{cases} \end{cases} \tag{21}$$

The Tresca transformation criterion can be defined as

$$\hat{\varphi}(\boldsymbol{\sigma}^{\mathbf{eff}}) = H^{\max} Max\{\left|\sigma_1^{eff} - \sigma_2^{eff}\right|, \left|\sigma_2^{eff} - \sigma_3^{eff}\right|, \left|\sigma_1^{eff} - \sigma_3^{eff}\right|\} \tag{22}$$

where $H^{\max}$ is the maximum transformation strain in a uniaxial stress test σ_1^{eff}, σ_2^{eff} and σ_3^{eff} are the real principle values of the symmetric second order tensor $\boldsymbol{\sigma}^{eff}$. Given $\boldsymbol{\sigma}^{\mathbf{eff}} = diag\{\sigma_{rr}^{eff}, \sigma_{\theta\theta}^{eff}, \sigma_{zz}^{eff}\}$ in the polar coordinate system and assuming $\sigma_{\theta\theta}^{eff} > \sigma_{zz}^{eff} > \sigma_{rr}^{eff}$ which can be the case for the special condition of an axisymmetric SMA cylinder under internal pressure, it follows that

$$\hat{\boldsymbol{\Phi}}(\boldsymbol{\sigma}^{\mathbf{eff}}) = H^{\max}(\sigma_{\theta\theta}^{eff} - \sigma_{rr}^{eff}) \tag{23}$$

And therefore from equation (20)

$$\frac{\partial\hat{\boldsymbol{\Phi}}(\boldsymbol{\sigma}^{\mathbf{eff}})}{\partial\boldsymbol{\sigma}^{\mathbf{eff}}} = H^{\max}\begin{bmatrix} -1 & 0 & 0 \\ 0 & +1 & 0 \\ 0 & 0 & 0 \end{bmatrix} \tag{24}$$

which means

$$\varepsilon_{zz}^t = 0, \quad \varepsilon_{\theta\theta}^t = -\varepsilon_{rr}^t \tag{25}$$

According to the Tresca transformation criterion, no transformation occurs in the axial direction for the axisymmetric SMA cylinder under internal pressure and also the transformation strains in the radial and circumferential directions have equal and opposite values. It is worth noting that this result is in accordance with the assumed volume-preserving nature of the phase transformation

$$\varepsilon_{zz}^t + \varepsilon_{\theta\theta}^t + \varepsilon_{rr}^t = 0 \tag{26}$$

The Tresca equivalent stress for the current problem is

$$\sigma_\theta - \sigma_r = \sigma_y^{fwd(rev)} \tag{27}$$

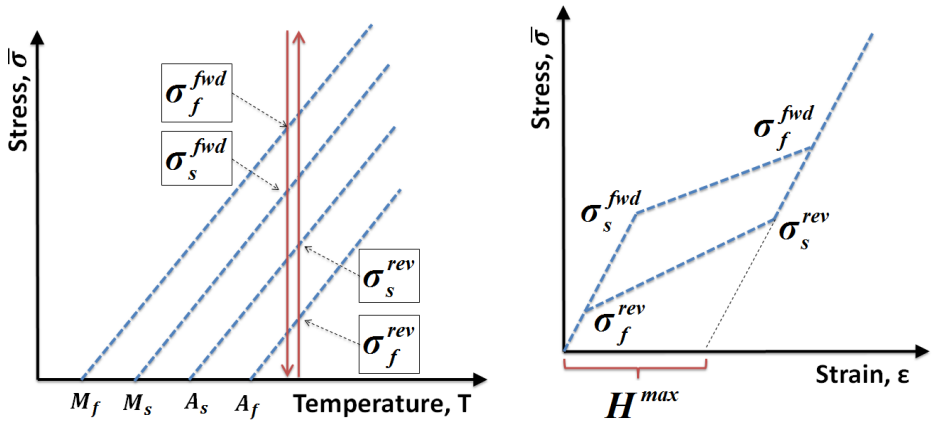

Figure 1: Schematic response of SMAs under a psuedoelastic loading and unloading path

It is well-known that under tensile loads, SMAs exhibit inhomogeneous deformations, and coupling the problem with temperature, of course, makes the solution even more complex. In order to get the analytical solution, a three dimensional constitutive model for the SMAs is provided that incorporates Tresca transformation criterion and flow rule allowing for linear hardening equations. The 1D isothermal pseudoelastic response of the SMA is schematically depicted in Fig. 1. As seen in Fig. 1 [Tabesh, Liu, Boyd and Lagoudas (2013)] the Tresca equivalent stress can be expressed that, during transformation,

$$\sigma_y^{fwd(rev)}(T) = \sigma_s^{fwd(rev)}(T) + \frac{\sigma_f^{fwd(rev)}(T) - \sigma_s^{fwd(rev)}(T)}{H^{\max}} \varepsilon_\theta^t \tag{28}$$

where$\sigma_s^{fwd}(T)$, $\sigma_f^{fwd}(T)$, $\sigma_s^{rev}(T)$, $\sigma_f^{rev}(T)$are the critical stresses for the start and finish of forward/reverse transformations in the SMAs and they are assumed as linear functions of temperature

$$\begin{aligned}
\sigma_s^{fwd}(T) &= C_M(T(r) - M_s) \\
\sigma_f^{fwd}(T) &= C_M(T(r) - M_f) \\
\sigma_s^{rev}(T) &= C_A(T(r) - A_s) \\
\sigma_f^{rev}(T) &= C_A(T(r) - A_f)
\end{aligned} \tag{29}$$

where M_s, M_f, A_s, A_f are the critical transformation temperatures, C_A, C_M are the

slopes of stress-temperature phase diagrams $T(r)$ is the temperature at the current point.

3 Thermal stresses in a thick-walled cylinder

3.1 Elastic analysis

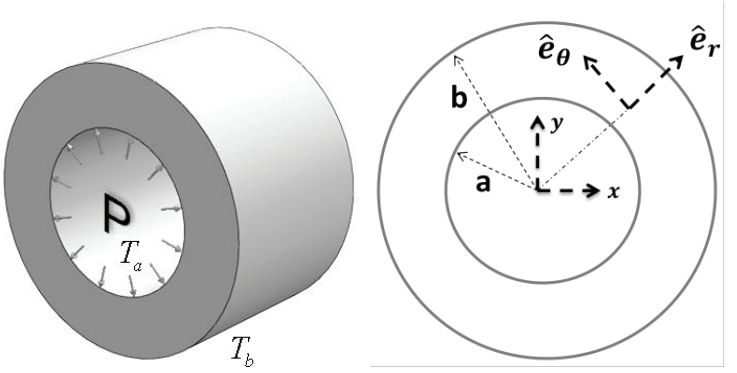

(a) (b)

Figure 2: The SMA cylinder under Internal pressure and radial temperature gradient

A state of axial symmetry is considered in the problem if an SMA cylinder under internal pressure and radial temperature gradient (Fig. 2a). The boundary conditions for the cylinder considered in this case, with inner radius $T = T_a$, $\sigma_r = -P$, $r = a$and outer radius $T = T_b$, $\sigma_r = 0$, $r = b$. It is assumed that the axial displacement, w (and therefore the axial strainε_{zz}), does not change through the thickness. Then the strain-displacement relations, assuming small displacement gradient in polar coordinates system, can be simplified. Similarly, the general form of equilibrium equations in polar coordinates can be reduced for axisymmetric conditions as shown in Fig. 2 (b). Then for the present problem, the strain-displacement relations and the equilibrium equations are given by

$$\begin{cases} \varepsilon_r = \dfrac{\partial u}{\partial r}, \varepsilon_\theta = \dfrac{u}{r}, \varepsilon_z = \dfrac{\partial w}{\partial z} \\ \dfrac{\partial \sigma_r}{\partial r} + \dfrac{1}{r}(\sigma_r - \sigma_\theta) = 0 \end{cases} \tag{30}$$

where σ_θ and σ_r are circumferential/tangential stress and radial stress, respectively.

ε_r, ε_θ and ε_z are the radial, tangential and axial strain, respectively. u is the displacement in the radial direction, r is the radial coordinate

If the coefficient of linear expansion is denoted by α, the dilatation produced by a rise in temperature T is equal to αT. It is assumed that the elastic modulus of martensite is equal to the austenite case, as $E = E_M = E_A$. Subtracting this from each strain component in the generalized Hooke's law, we have the elastic stress-strain equations:

$$\begin{cases} \varepsilon_r^- \alpha T = \dfrac{1}{E}\left(\sigma_r - \upsilon\left(\sigma_\theta + \sigma_z\right)\right) \\ \varepsilon_\theta^- \alpha T = \dfrac{1}{E}\left(\sigma_\theta - \upsilon\left(\sigma_r + \sigma_z\right)\right) \\ \varepsilon_z^- \alpha T = \dfrac{1}{E}\left(\sigma_z - \upsilon\left(\sigma_r + \sigma_\theta\right)\right) \end{cases} \tag{31}$$

where υ is the poisson's ratio and σ_z is the axial stress

Algebraic manipulation of the above equations results in

$$\begin{cases} \dfrac{\partial u}{\partial r} = -\upsilon\varepsilon_z + (1+\upsilon)\alpha T + \dfrac{(1+\upsilon)}{E}\left((1-\upsilon)\sigma_r - \upsilon\sigma_\theta\right) \\ \dfrac{u}{r} = -\upsilon\varepsilon_z + (1+\upsilon)\alpha T + \dfrac{(1+\upsilon)}{E}\left((1-\upsilon)\sigma_\theta - \upsilon\sigma_r\right) \end{cases} \tag{32}$$

for a linear elastic cylinder. Also, under the 2D plane conditions

$$\begin{cases} \varepsilon_z = -\dfrac{\upsilon}{E}(\sigma_r + \sigma_\theta);\ \sigma_z = 0 \qquad for\ plane\ stress \\ \sigma_z = \upsilon\left(\sigma_r + \sigma_\theta\right); \quad \varepsilon_z = 0 \qquad for\ plane\ strain \end{cases} \tag{33}$$

If we assume a steady state distribution of temperature, T satisfies the Laplace equation $\nabla^2 T = 0$, the solution of which may be written as

$$T(r) = T_b + (T_a - T_b)\frac{\ln(b/r)}{\ln(b/a)} \tag{34}$$

where T_a and T_b are the temperatures at the inner and the outer surfaces respectively. It is convenient at this stage to introduce a dimensionless parameter β defined as

$$\beta = \frac{\alpha(T_a - T_b)}{2(1-\upsilon)} \tag{35}$$

The elastic analysis for the model can be easily got by elasticity with the boundary conditions. The following expressions can be obtained

$$\begin{cases} \sigma_r = -(P - \beta E)\left(\dfrac{b^2}{r^2} - 1\right)\left(\dfrac{b^2}{a^2} - 1\right)^{-1} - \beta E\dfrac{\ln(b/r)}{\ln(b/a)} \\ \sigma_\theta = (P - \beta E)\left(\dfrac{b^2}{r^2} + 1\right)\left(\dfrac{b^2}{a^2} - 1\right)^{-1} + \beta E\dfrac{1 - \ln(b/r)}{\ln(b/a)} \end{cases} \tag{36}$$

When P and β are increased to critical values, yielding may begin anywhere in the cylinder depending on the ratio of these parameters. We shall be concerned here with the situation where σ_z is the intermediate principal stress in the element that yields. If Tresca's yield criterion is adopted, yielding will depend on the magnitude of the stress difference

$$\sigma_\theta - \sigma_r = (P - \beta E)\frac{2b^2/r^2}{b^2/a^2 - 1} + \frac{\beta E}{\ln(b/a)} \tag{37}$$

The yield function can be obtained as

$$\begin{aligned} F(r) =& (P - \frac{\alpha(T_a - T_b)}{2(1-\upsilon)}E)\frac{2b^2/r^2}{b^2/a^2 - 1} + \frac{\alpha(T_a - T_b)E}{2(1-\upsilon)\ln(b/a)} \\ & - C_M T_b + C_M M_s - C_M(T_a - T_b)\frac{\ln(b/r)}{\ln(b/a)} \end{aligned} \tag{38}$$

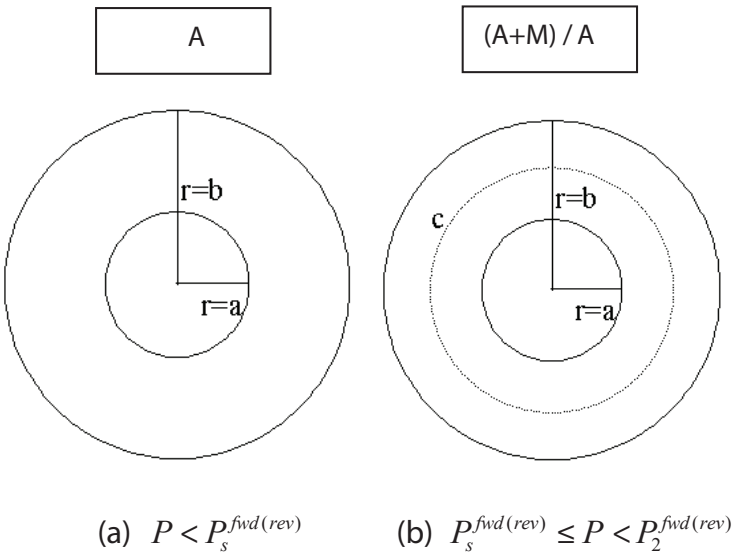

Figure 3: Transformation distributions of the SMA cylinder

The loading of the internal pressure occurs in elastic and transformation steps with regards to the martensitic transformation, as schematically shown in Fig.3. The SMA cylinder is assumed to be at a homogeneous temperature $T_b > T_a > A_f$, thus it is initially fully austenitic as seen in Fig. 3 (a). According to (38), as the pressure increases, the Tresca equivalent stress also increase, with the maximum being at

the inner radius, $r = a$. Therefore, the transformation to martensite starts at the inner radius as soon as the Tresca criterion $\sigma_\theta - \sigma_r|_{r=a} = \sigma_s^{fwd}$, then the yielding begining pressure is obtained as

$$P_s^{fwd} = \beta E - \frac{\beta E}{2\ln(b/a)}(1-\frac{a^2}{b^2}) + \frac{1}{2}(C_M T_b - C_M M_s + C_M(T_a - T_b)\frac{\ln(b/r)}{\ln(b/a)})(1-\frac{a^2}{b^2}) \tag{39}$$

So when internal pressure $P < P_s^{fwd}$, the stress distribution can be obtained by (36) and the martensite volume fraction $\xi = 0$

3.2 Analysis of forward transformation

Futher increase in the pressure results in propagation of the forward transformation front, denoted by $r = c$, through the thickness of the cylinder as seen in Fig. 3 (b). At a pressure between $P_s^{fwd} \le P < P_2^{fwd}$, the cylinder consists of an inner ring, which has a mixture of martensite and austenite ($1 \ge \xi \ge 0 a \le r \le c$), and an outer ring, which is completely austenite ($\xi = 0 c < r < b$). For this case, the pressure P_2^{fwd} denotes the finish critical pressure of the step when the inner radius is completely transformed to martensite.

Combining the kinematic equations Hook's law (32), the equilibrium equation (30), the total strain can be expressed as

$$\frac{du}{dr} + \frac{u}{r} = -2\upsilon\varepsilon_z + \frac{1-2v}{2G}\frac{1}{r}\frac{d}{dr}(r^2\sigma_{rr}) + 2(1+\upsilon)\alpha T(r) \tag{40}$$

where $G = E/(2+2v)$. This differential equation is valid throughout the cylinder, the transforming inner ring and the elastic outer ring as schematically shown in Fig. 3(b)

The outer ring $c < r \le b$ is elastic austenite. Thus, the problem can be solved using Lame's solution and the boundary conditions $\sigma_r(c) = -P_c,\ \sigma_\theta - \sigma_r|_{r=c} = \sigma_s^{fwd}$ Therefore

$$\begin{cases} \sigma_r = -(P_c - \beta E)(\dfrac{b^2}{r^2} - 1)(\dfrac{b^2}{c^2} - 1)^{-1} - \beta E\dfrac{\ln(b/r)}{\ln(b/c)} \\ \sigma_\theta = (P_c - \beta E)(\dfrac{b^2}{r^2} + 1)(\dfrac{b^2}{c^2} - 1)^{-1} + \beta E\dfrac{1-\ln(b/r)}{\ln(b/c)} \end{cases} \tag{41}$$

$$P_c = \beta E - \frac{\beta E}{2\ln(b/a)}(1-\frac{c^2}{b^2}) + \frac{1}{2}(C_M T_b - C_M M_s + C_M(T_a - T_b)\frac{\ln(b/r)}{\ln(b/a)})(1-\frac{c^2}{b^2})$$

(42)

The radial displacement at the outer surface, $u(b)$, can be found from (32). This enables one to integrate equation (40) from a point within the cylinder to the outer radius where the radial stress and displacement are known, that is

$$\frac{u}{r} = -\upsilon\varepsilon_z + (1+\upsilon)\alpha T + \frac{(1+\upsilon)}{E}\left(\frac{(P_c-\beta E)(b^2/r^2+1-2\upsilon)}{b^2/c^2-1} + \frac{\beta E(1-\upsilon)+(2\upsilon-1)\beta E\ln(b/r)}{\ln(b/c)}\right) \tag{43}$$

$$u(b) = -b\upsilon\varepsilon_z + (1+\upsilon)b^2\alpha T_b + b\frac{(1+\upsilon)}{E}\left(\frac{2(P_c-\beta E)(1-\upsilon)}{b^2/c^2-1} + \frac{\beta E(1-\upsilon)}{\ln(b/c)}\right) \tag{44}$$

$$\frac{(ru)'}{r} = \frac{\partial u}{\partial r} + \frac{u}{r} = -2v\varepsilon_z + \frac{1-2v}{2G}\frac{1}{r}\frac{\partial(r^2\sigma_r)}{\partial r} + 2(1+\upsilon)\alpha T(r) \tag{45}$$

Then

$$(ru)' = -2rv\varepsilon_z + \frac{1-2v}{2G}\frac{\partial(r^2\sigma_r)}{\partial r} + 2(1+\upsilon)\alpha rT(r) \tag{46}$$

$$ru\big|_b^r = -r^2v\varepsilon_z\big|_b^r + \frac{1-2v}{2G}r^2\sigma_r\Big|_b^r + 2(1+\upsilon)\alpha\int_b^r rT(r)dr \tag{47}$$

$$\begin{aligned} ru - bu(b) = &-r^2v\varepsilon_z + \frac{1-2v}{2G}r^2\sigma_r + 2(1+\upsilon)\alpha\{\frac{1}{2}r^2T_b - \frac{(T_a-T_b)r^2}{4\ln(b/a)}]\} \\ &+ b^2v\varepsilon_z - \frac{1-2v}{2G}b^2\sigma_r(b) - 2(1+\upsilon)\alpha\{\frac{1}{2}b^2T_b - \frac{(T_a-T_b)b^2}{4\ln(b/a)}]\} \end{aligned} \tag{48}$$

Combining (44) and (48) this leads to

$$ru = -r^2v\varepsilon_z + \frac{1-2v}{2G}r^2\sigma_r + 2(1+\upsilon)\alpha\{\frac{1}{2}r^2T_b - \frac{(T_a-T_b)r^2}{4\ln(b/a)}]\} + K \tag{49}$$

where

$$\begin{aligned} K =&(1+\upsilon)b^2\alpha T_b + b^2\frac{(1+\upsilon)}{E}[\frac{2(P_c-\beta E)(1-\upsilon)}{b^2/c^2-1} + \frac{\beta E(1-\upsilon)}{\ln(b/c)}] \\ &- 2(1+\upsilon)\alpha[\frac{1}{2}r^2T_b - \frac{(T_a-T_b)r^2}{4\ln(b/a)}] \end{aligned} \tag{50}$$

Then the total strain can be obtained by

$$\varepsilon_\theta = \frac{u}{r} = -v\varepsilon_z + \frac{1-2v}{2G}\sigma_r + 2(1+\upsilon)\alpha\{\frac{1}{2}T_b - \frac{(T_a-T_b)}{4\ln(b/a)}]\} + \frac{K}{r^2} \tag{51}$$

Then the transformation strain $\varepsilon_\theta^t = \varepsilon_\theta - \varepsilon_\theta^e$ can be got by

$$\varepsilon_\theta^t = \frac{1-v}{2G}(\sigma_r - \sigma_\theta) + 2(1+\upsilon)\alpha\{\frac{1}{2}T_b - \frac{(T_a-T_b)}{4\ln(b/a)}]\} - (1+\upsilon)\alpha T(r) + \frac{K}{r^2} \tag{52}$$

Considering the Tresca's yield function (28), the transformation strain can be expressed as

$$\varepsilon_\theta^t = \frac{-\frac{1-v}{2G}\sigma_s^{fwd} + 2(1+\upsilon)\alpha\{\frac{1}{2}T_b - \frac{(T_a-T_b)}{4\ln(b/a)}]\} - (1+\upsilon)\alpha T(r) + \frac{K}{r^2}}{1+A} \tag{53}$$

where $A = \frac{1-\upsilon^2}{E}\frac{(\sigma_f^{fwd}-\sigma_s^{fwd})}{H^{\max}}$.
According to (28), (30) and (53), the response can be given by

$$\frac{\partial\sigma_r}{\partial r} = \frac{1}{r}[\sigma_s^{fwd} + \frac{\sigma_f^{fwd}-\sigma_s^{fwd}}{H}\frac{-\frac{1-v}{2G}\sigma_s^{fwd} + 2(1+\upsilon)\alpha\{\frac{1}{2}T_b - \frac{(T_a-T_b)}{4\ln(b/a)}]\} - (1+\upsilon)\alpha T(r) + \frac{K}{r^2}}{1+A}] \tag{54}$$

Integrating the function (54) leads to

$$\int_c^r \frac{\partial\sigma_r}{\partial r}dr = \sigma_r(r) - \sigma_r(c) = F\ln r\Big|_c^r + \frac{1}{2}(\ln r)^2 B\Big|_c^r - \frac{1}{2}\frac{K(C_mM_s - C_mM_f)}{H(1+A)}r^{-2}\Big|_c^r \tag{55}$$

where

$$F = \frac{C_MT_b - C_MM_s + C_M(T_a-T_b)\ln b}{1+A} + \frac{C_MM_s - C_MM_f}{H(1+A)}\alpha(1+\upsilon)[T_b - \frac{(T_a-T_b)(4\ln b+1)}{2\ln(b/a)}]$$

$$B = \frac{-C_M(T_a-T_b)}{1+A} + \frac{C_MM_s - C_MM_f}{H(1+A)}2\alpha(1+\upsilon)\frac{(T_a-T_b)}{\ln(b/a)}$$

where $\sigma_r(c)$ can be got by (41) Therefore

$$\sigma_r(r) = F\ln\frac{r}{c} + \frac{1}{2}B[(\ln r)^2 - (\ln c)^2] - \frac{1}{2}\frac{K(C_mM_s - C_mM_f)}{H(1+A)}(\frac{1}{r^2} - \frac{1}{c^2}) + \sigma_r(c)$$

$$\sigma_\theta(r) = \sigma_r(r) + \sigma_s^{fwd} + \frac{(C_mM_s - C_mM_f)}{H}\frac{-\frac{1-v}{2G}\sigma_s^{fwd} + 2(1+\upsilon)\alpha\{\frac{1}{2}T_b - \frac{(T_a-T_b)}{4\ln(b/a)}]\} - (1+\upsilon)\alpha T(r) + \frac{K}{r^2}}{1+A}$$

(56)

The critical radius c_{cr} and the critical pressure P_2^{fwd} can be obtained by using the boundary conditions $\sigma_\theta - \sigma_r|_{r=a} = \sigma_f^{fwd}$ and $\sigma_\theta - \sigma_r|_{r=c} = \sigma_s^{fwd}$

4 Numerical results

The analytical results for plane strain are discussed in this section. The structural response of the SMA cylinder depends on the radial temperature gradient and internal pressure as well as material properties and geometry. Therefore, the following groups are given for loading of the cylinder: the internal radius $a = 10mm$ the external radius $b = 30mm$, the radial temperature gradient from internal radius $T_a = 60^\circ C$ to the outer radius$T_b = 100^\circ C$. The material parameters controlling the response of the structure plotted in this section are given in table 1.

Table 1: Parameters used in calculation for SMA cylinder [Tablesh, Atli, Rohmer, Franco, Karaman, Boyd and Lagoudas (2012)]

v	E	C_M	M_s	M_f	A_s	A_f	α	$H_{\max}$	T_a	T_b
0.4	85Gpa	$10MPa/^\circ C$	-50$^\circ C$	-70$^\circ C$	40$^\circ C$	60$^\circ C$	0.00001	0.032	60$^\circ C$	100$^\circ C$

The numerical results by finite element (FE) program (ANSYS) of SMA cylinder under combined internal pressure and radial temperature gradient are presented in this part. Considering symmetry, the FE program can be applied to a 1/4 part of the cylinder with the fixed constraints at both x direction and y direction. The FE model is described in Fig. 4 and the stresses and martensite volume fractions, obtained numerically with FE program are presented in the following figures.

Fig. 5 demonstrates the thermo-elastic stress components through the thickness of the cylinder under internal pressure $P = 100Mpa$ with the radial temperature gradient from $T_a = 60^\circ C$ to $T_b = 100^\circ C$. As seen in Fig. 5 the numerical results are in good agreement with the FE results, and all the thermo-elastic stresses are continuous.

Fig. 6 shows the plot of thermo-elastic stress distributions through the thickness of the SMA cylinder under the internal pressure $P = 100Mpa$ and the varying radial temperature gradient from $T_a = 60^\circ C$ to different values of $T_b(60^\circ C, 80^\circ C, 100^\circ C)$. As seen in Fig. 6 (a), the circumferential stresses have descending distributions through the thickness of the SMA cylinder There is a positive effect on the circumferential stresses at the inner part ($r \leq 18mm$) of the cylinder by the increasing values of T_b, and shows a negative effect at the outer part ($r \geq 18mm$). As seen in Fig. 6 (b), the radial stresses decrease with increasing values of T_b.

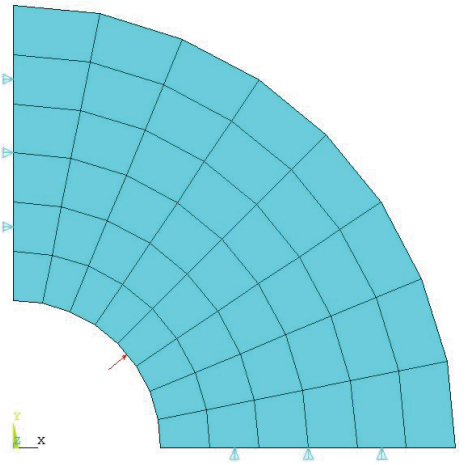

Figure 4: Transformation distributions of the SMA cylinder

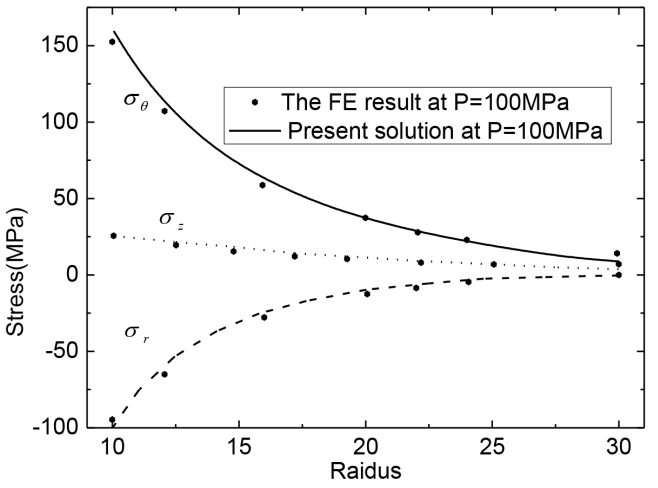

Figure 5: Thermo-elastic stress distribution for the SMA cylinder under the internal pressure $P = 100Mpa$ and the radial temperature gradient $T_a = 60°C$, $T_b = 100°C$

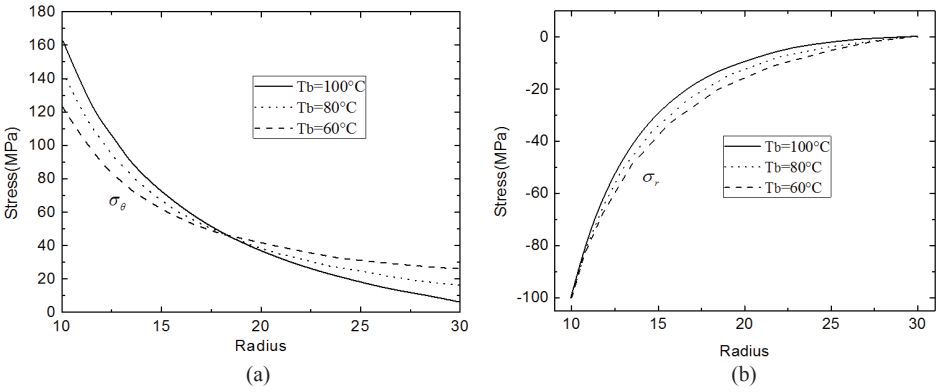

Figure 6: Thermo-elastic stress distribution for the SMA cylinder under the internal pressure $P = 100Mpa$ and the radial temperature gradient from $T_a = 60°C$ to different T_b

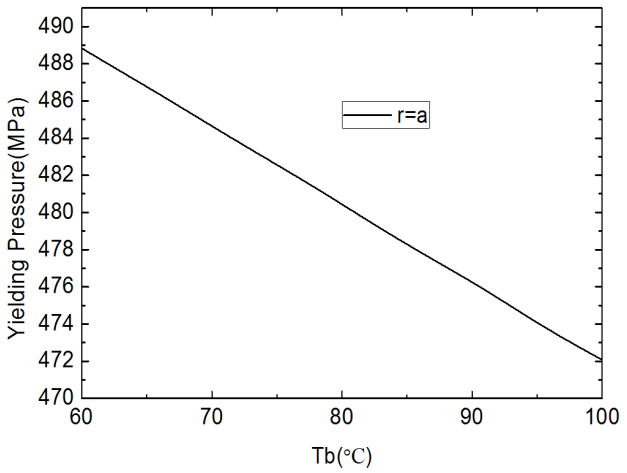

Figure 7: The yielding beginning internal pressures for the SMA cylinder under the radial temperature gradient with constant $T_a = 60°C$ and changing T_b from $60°C$ to $100°C$

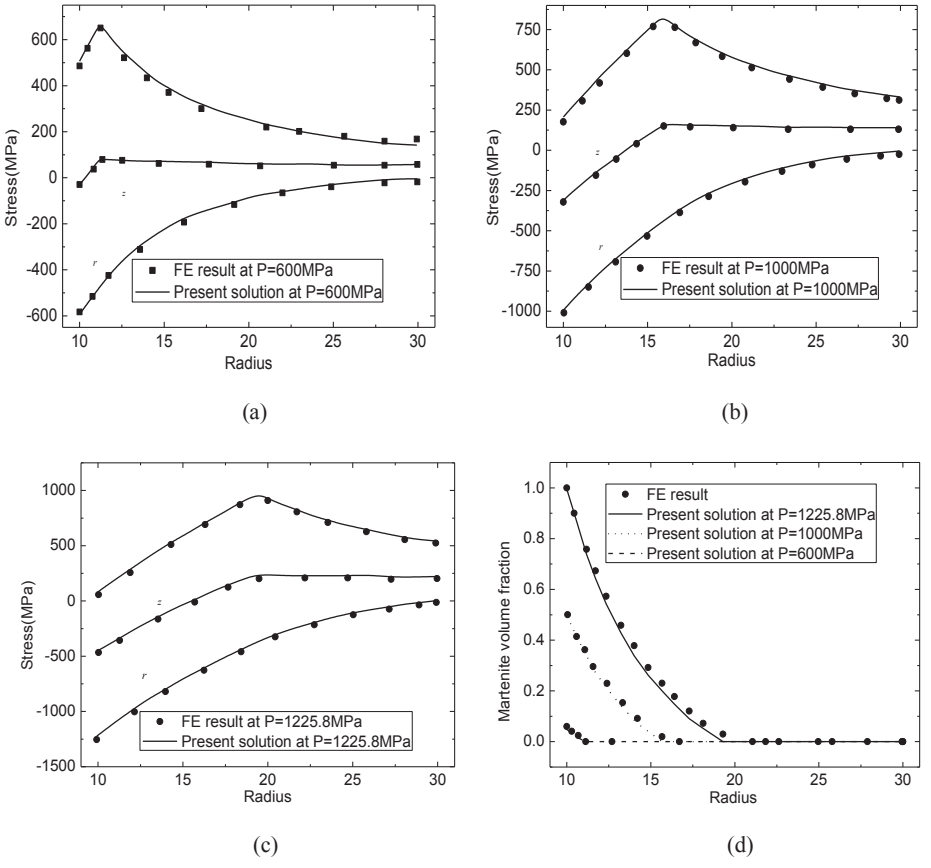

Figure 8: Distribution of the stresses and martenite volume fraction for the SMA cylinder under the radial temperature gradient $T_a = 60°C$, $T_b = 100°C$ and different inner pressures.

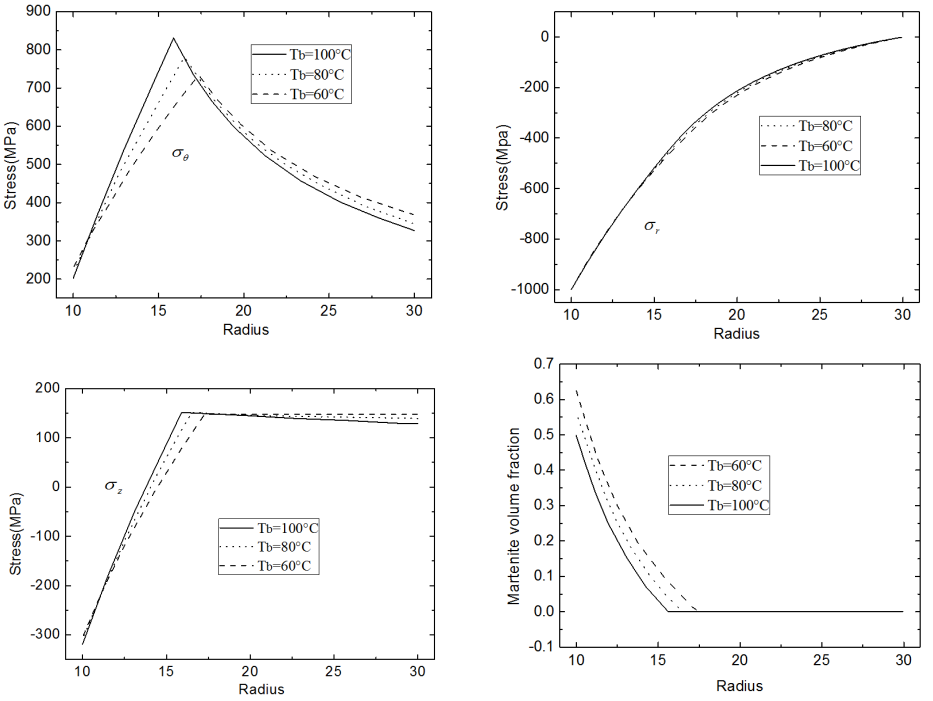

Figure 9: Distribution of the stresses and martenite volume fraction for the SMA cylinder under P=1000MPa and the radial temperature gradient from $T_a = 60°C$ and to different T_b

The yielding beginning internal pressure of this model can be calculated by (39). With constant $T_a = 60°C$ and changing T_b from $60°C$ to $100°C$, the different values of the corresponding pressures can be shown in Fig. 7 As seen in the Fig. 7, the yielding beginning internal pressures decrease with the increasing values of T_b.

Fig. 8 shows the stress and the martensite volume fraction distributions through the thickness of the SMA cylinder under different inner pressures P=600, 1000, 1228.5MPa and the radial temperature gradient from $T_a = 60°C$ to $T_b = 100°C$. As seen in Fig. 8 (a-c), the body of the cylinder is composed of an inner transforming region and an outer elastic region. The circumferential stress and the axial stress components have ascending distributions in the inner transforming region and follow descending distributions in the outer elastic region. The highest circumferential stress occurs at the interface between the transforming and elastic regions. Martensitic volume fraction distributions, calculated by the present method, are shown

in Fig. 8 (d) The numerical results show good agreement with the finite element results.

Fig. 9 shows the stress and the martensite volume fraction distributions through the thickness of the SMA cylinder under the inner pressure P=1000MPa and varying radial temperature gradient from $T_a = 60°C$ to different values of $T_b(60°C, 80°C, 100°C)$. As seen in Fig. 9 (a-c), different stress components are obtained There is a positive effect on the circumferential and axial stresses by the increasing values of T_b in the outer elastic region of the cylinder, and shows a negative effect in the inner transforming region For the radial stresses, the distributions are nearly the same. The martensitic volume fraction distributions, which are shown in Fig. 9 (d), decrease with the increasing values of T_b.

5 Conclusions

An analytical model were provided for the circumferential stress, radial stress, and martensite volume fraction of a pseudoelastic SMA thick-walled cylinder subjected to internal pressure and radial temperature gradient. The SMA constitutive model was derived using a free-energy function and a Tresca-based transformation criterion. It was shown that the stress distributions and the martensite volume fraction distributions can be substantially decreased or increased depending on both increasing internal pressures and varying temperature fields. There was a good agreement between the analytical results and the FE numerical results. The analytical solution can provide an effective engineering tool to predict the deformation response of such components and design mechanism, such as actuators, which require high controllability.

Acknowledgement: The authors acknowledge the financial support of National Natural Science Foundation of China (No. 11132003, 11172033, 11272044 and 11272136) and National Basic Research Program of China (973 Program) (2010CB 7321004) and it is also supported by "the scientific research foundation of civil aviation university of China (2013QD08S)" The authors are also very grateful to Dr. Lagoudas Dr. Boyd and Dr. Tabesh Texas A&M University, USA, for their helpful suggestions.

References

Auricchio, F.; Conti, M.; Morganti, S.; Reali, A. (2010): Shape memory alloy: From constitutive modeling to finite element analysis of stent deployment. *CMES: Computer Modeling in Engineering and Sciences*, vol. 53 no. 3, pp 225-244.

Boyd, J. G.; Lagoudas, D. C. (1996): A thermodynamic constitutive model for

the shape memory alloy materials. Part I. the monolithic shape memory alloy. *Int. J. Plast.* vol. 12 pp. 805–842.

Chen, B.; Peng, X.; Chen, X.; Wang, J.; Wang, H.; Hu, N. (2012): A Three-Dimensional Model of Shape Memory Alloys under Coupled Transformation and Plastic Deformation. *CMC: Computers Materials and Continua*, vol. 30, no. 2, pp. 145176.

Feng, X. Q.; Sun, Q. P. (2007): In situ profilometry for non-uniform strain field measurement of NiTi shapememory alloymicrotubing under complex stress states. *Smart Mater. Struct.* vol. 16, no. 1 pp. 179–186.

Garner, L. J.; Wilson, L. N.; Lagoudas, D. C.; Rediniotis, O. K. (2000): Development of a shape memory alloy actuated biomimetic vehicle. *Smart Mater. Struct.* vol. 9 pp. 673–683.

Gyunter, V. E.; Sysoliatin, P.; Temerkahamor, T. (1995): *Superelastic shape memory implants in maxillofacial surgery, traumatology, orthopedics, and neurosurgery.* Tomsk university publishing house, Tomsk.

He, Y. J.; Sun, Q. P. (2009): Scaling relationship on macroscopic helical domains in NiTi tubes. *Int. J. Solids Struct*., vol. 46 pp. 4242–4251.

Ilyin, A.; Dudin, M.; Makarova, I. (1995): NiTi instruments for TMJ surgeries. In: Conf. Proc. Superelastic shape memory Implants in Medicine. Tomsk, pp. 61-62.

Jee, K. K.; Hana, J. H.; Jang, W. Y. (2006): A method of pipe joining using shape memory alloys. *Mater. Sci. Eng. A*., vol. 438, no. 440 pp. 1110–1112.

Kim, C.; Jang, D. H.; Choi, H. S. (2002): An externally pressurized elliptic composite cylinder stiffened with activated SMA strips. *In: 43rd AIAA/ASME/ASCE/AHS/ASC Structures, Structural Dynamics, and Materials Conference*, pp. 22–25. Denver, Colorado.

Kuribayashi, K.; Tsuchiya, K.; You, Z.; Tomusb, D.; Umemotob, M.; Ito, T.; Sasaki, M. (2006): Self-deployable origami stent grafts as a biomedical application of Ni-rich TiNi shape memory alloy foil. *Mater. Sci. Eng. A*., vol. 419 pp. 131–137.

Lagoudas, D. C.; Bo, Z.; Qidwai, M. A. (1996): A unifed thermodynamic constitutive model for SMA and finite element analysis of active metal matrix composite. *Mech. Compos. Mater. Struct*., vol. 3 pp. 153–179.

Langelaar, M.; Keulen, F. V. (2004): Modeling of a shape memory alloy active catheter. *In: 45th AIAA Structures, Structural Dynamics and Materials Conference,* pp. 19–22. Palm Springs, Calofornia.

Li, Z. Q.; Sun, Q. P. (2002): The initiation and growth of macroscopic martensite

band in nano-grained NiTi microtube under tension. *Int. J. Plast*., vol. 18 pp. 1481–1498.

Liang, C.; Davidson, F.; Scjetky, L. M.; Straub, F. K. (1996): Applications of torsional shape memory alloy actuators for active rotor blade control: opportunities and limitations. *In: SPIE Proc. Mathematics and Controls in Smart Structures* vol. 2717, pp. 91-100.

Liu, B. F.; Dui, G. S.; Zhu, Y. P. (2011): A constitutive model for porous shape memory alloys considering the effect of hydrostatic stress. *CMES-Comp. Model. Eng.,* vol. 78 no. 4 pp. 247-275.

Liu, B. F; Dui, G. S; Zhu, Y. P. (2012): On phase transformation behavior of porous shape memory alloy. *J. Mech. Behav. Biomed.* vol. 5 pp. 9-15.

Machado, L. G.; Savi, M. A. (2003): Medical applications of shape memory alloys. *Braz. J. Med. Biol. Res*., vol. 36 pp. 683–691.

Martynova, I.; Skorohod, V.; Solonin, S.; Goncharuk, S. (1991): Shape memory and superelasticity behaviour of porous Ti-Ni material. *J. Phys. IV*., vol. 1, pp. 421-426.

Mirzaeifar, R.; Shakeri, M.; DesRoches, R.; Yavari, A. (2011): A semi-analytic analysis of shape memory alloy thick-walled cylinders under internal pressure. *Arch Appl Mech*., vol. 81 pp. 1093–1116.

Müller, I.; Seelecke, S. (2001): Thermodynamic aspects of shape memory alloys. *Math. Comput. Model*, vol. 34, no. 12-13 pp. 1307–1355.

Müller, I.; Xu, H. (1991): On the pseudo-elastic hysteresis. *Acta Metal. Mater*., vol. 39, no. 3 pp. 263–271.

Paine, J. S. N.; Rogers, C. A.; Smith, R. A. (1995): Adaptive composite-materials with shape-memory alloy actuators for cylinders and pressure-vessels. *J. Intell. Mater. Syst. Struct*., vol. 6, no. 2 pp, 210–219.

Qidwai, M. A.; Lagoudas, D. C (2000): On thermomechanics and transformation surfaces of polycrystalline NiTi shape memory alloy material. *Int. J. Plast*., vol. 16, pp. 1309–1343.

Tabesh, M.; Atli, K. C.; Rohmer, J.; Franco, B. E.; Karaman, I.; Boyd, J. G.; Lagoudas, D. C. (2012): Design of shape memory alloy pipe couplers: modeling and experiments. *Industrial and Commercial Applications of Smart Structures Technologies Proc. of SPIE,* vol. 8343, 83430J.

Tabesh, M.; Liu, B. F.; Boyd, J.; Lagoudas, D. C. (2013): Analytical Solution for pseudoelastic response of a shape memory thick-walled cylinder under interal pressure. *Smart Mater. Struct* vol. 22, 094007.

Xua, M. B.; Song, G. (2004): Adaptive control of vibration wave propagation in

cylindrical shells using SMA wall joint. *J. Sound Vib*., vol. 278 pp. 307326.